Inter-Particle Electronic and Ionic Modifications of the Ternary Ni-Co-Mn Oxide for Efficient and Stable Lithium Storage

Yanbin Zhu,[1] Yingke Zhou,[1,z] Xiaohui Tian,[1] Xiao Huang,[1] Runqi Yu,[1] Guan Wu,[1] and George Z. Chen[1,2]

[1] *The State Key Laboratory of Refractories and Metallurgy, Institute of Advanced Materials and Nanotechnology, College of Materials and Metallurgy, Wuhan University of Science and Technology, Wuhan 430081, China*
[2] *Energy Engineering Research Group, Faculty of Science and Engineering, University of Nottingham Ningbo China, Ningbo 316100, China*

A combined electronic and ionic interparticular modification strategy is designed for the improvement of lithium storage in the layer structured ternary Ni-Co-Mn oxide ($LiNi_{0.6}Co_{0.2}Mn_{0.2}O_2$) in the form of spherical particles. In this design, a thin layer of the ion conducting polypropylene carbonate is applied to wrap the individual oxide particles for three purposes: (1) prevention of direct stacking and packing between oxide particles that will otherwise impede or block ions from accessing all the surface of the oxide particles, (2) provision of additional ionic pathways between the oxide particles, and (3) stabilization of the oxide particles during lithium storage and release. The design includes also the use of nitrogen doped carbon nanotubes for electronic connection between the polymer coated individual spheres of the layered nickel-rich $LiNi_{0.6}Co_{0.2}Mn_{0.2}O_2$. According to the physicochemical and electrochemical characterizations, and laboratory battery tests, it can be concluded that the $LiNi_{0.6}Co_{0.2}Mn_{0.2}O_2$ composite has a unique porous structure that is assembled by the polymer coated ternary oxide microspheres and the nitrogen-doped carbon nanotube networks. Significant improvements are achieved in both the ionic and electronic conductivities (double or more increase), and in discharge specific capacity (201.3 $mAh{\cdot}g^{-1}$ at 0.1 C, improved by 13.28% compared to the non-modified $LiNi_{0.6}Co_{0.2}Mn_{0.2}O_2$), rate performance and cycling stability (94.40% in capacity retention after 300 cycles at 1.0 C).
 [DOI: 10.1149/2.0111914jes]

Manuscript submitted June 13, 2019; revised manuscript received August 26, 2019. Published September 18, 2019.

Lithium-ion batteries (LIBs) are widely applied in the daily life and the 3C products for their advantages of high energy density, excellent cycling performance and environmental friendliness.[1–4] Electrode materials are a key component of LIBs, and the development of high capacity positive electrode materials is imminent due to the increased requirements of energy/power density for the forthcoming wide application of electric vehicles. A particularly interesting example is a range of layer structured nickel-rich oxides of $LiNi_{1-x-y}Co_xMn_yO_2$ ($x + y \leq 0.5$), which possess relatively higher energy density compared to the widely used $LiCoO_2$ and $LiNi_{1/3}Co_{1/3}Mn_{1/3}O_2$ electrode materials.[5–8] However, these nickel-rich oxides usually display poor cycle life and rate performance because of the structure and thermal instability and the low electronic and ionic conductivities against the electrode reactions.[2,9,10] To overcome these shortcomings, various doping and surface modifications have been developed. For example, coating the particulates of $LiNi_{1-x-y}Co_xMn_yO_2$ with inorganic materials such as Al_2O_3, ZrO_2, CeO_2, MgO, Co_3O_4, TiO_2 or $LaPO_4$ was reported to be effective in resisting the attack of HF, reducing the side effects, and increasing the specific capacity and cycling stability.[11–17] The initial specific discharge capacity of the 5-nm TiO_2 coated $LiNi_{0.8}Co_{0.15}Al_{0.05}O_2$ particulates was found to be 189.9 $mAh{\cdot}g^{-1}$ at 1.0 C, and the retention was 90.2% after 100 cycles.[16] Similarly, the 4 wt%-$LaPO_4$ coated $LiNi_{0.5}Co_{0.2}Mn_{0.3}O_2$ retained 95.2% of its initial discharge capacity of 144.8 $mAh{\cdot}g^{-1}$ at 1.0 C after 100 cycles.[17] However, these inorganic coatings usually behave as an inert layer regarding ionic conduction, and tend to be discontinuously deposited onto the surface, leading to a limited coverage of the active materials.

Modification of the parent electroactive materials with a conductive polymer was found to be advantageous for coating uniformity and ion accessibility.[18–22] For instance, the lithium inserted ternary oxide, $LiNi_{0.6}Co_{0.2}Mn_{0.2}O_2$ (NCM622), displayed an initial discharge capacity of 171.3 $mAh{\cdot}g^{-1}$ at 0.5 C and a capacity retention of 93.5% after 100 cycles after modification with the poly(3,4-ethylenedioxythiophene)-co-poly(ethylene glycol) (PEDOT-co-PEG).[22] Among a wide variety of conductive polymers, poly(propylene carbonate) (PPC) seems to be more promising because of its demonstrated excellent conductivity to lithium ions through the mechanism of crystal vacancy diffusion.[23] However, PPC is not electronically conductive and should be used together with electronically conductive materials for more balanced and efficient electronic kinetics. In this line, graphene and carbon nanotube, particularly those doped with nitrogen could assist not only electron conduction, but also electrolyte wetting and affinity.[24,25]

In this work, a novel combined strategy of inter-particular ionic and electronic modifications is proposed for performance improvement of electroactive materials in general, and demonstrated using the spherical particulates of the layer structured $LiNi_{0.6}Co_{0.2}Mn_{0.2}O_2$ (NCM622) in the positive electrode of LIB as a particular example. The NCM622 powder was first prepared by a co-precipitation technique, and was then coated with a thin layer of PPC which would play three roles. It improves the ionic conductivity of the active material, decreases the occurrence of surface side reactions, and prevents agglomeration of the active particles which otherwise would reduce the effective contact area between the electrolyte and electroactive material. The PPC coated NCM622 particles were further modified with nitro-gen-doped carbon nanotubes (NCNT) by a dispersing and freeze drying process, leading to the production of the final composite for making the positive electrode. Compared to the unmodified materials, the NCNT and PPC dual-modified NCM622 (p-NCM622/NCNT) demonstrates greatly increased discharge specific capacity, rate performance and cycle stability, promising desirable capacity, power and durability improvement in LIBs.

Experimental

Preparation of materials.—The $Ni_{0.6}Co_{0.2}Mn_{0.2}(OH)_2$ precursor was synthesized by a co-precipitation method. $CoSO_4$, $MnSO_4$ and $NiSO_4$ (2:2:6, molar ratio) were dissolved in deionized water to obtain a 1.5 M solution of the metal ions. The solution was pumped into a continuously stirred tank (capacity 1.0 L) at a flow rate of 2 rpm using a peristaltic pump under argon. In the meantime, solutions of 0.9 M $NH_3{\cdot}H_2O$ and 4.0 M NaOH were separately pumped into the reactor at such rates that the pH of the mixture was maintained. The pH, temperature and stirring speed were set at 11.2, 55°C and 400 rpm, respectively. After reaction for 25 h, the precipitate was filtered and repeatedly washed with deionized water to remove the residual ions, followed by drying in an oven at 80°C for 24 h. The obtained hydroxide

[z]E-mail: zhouyk@wust.edu.cn

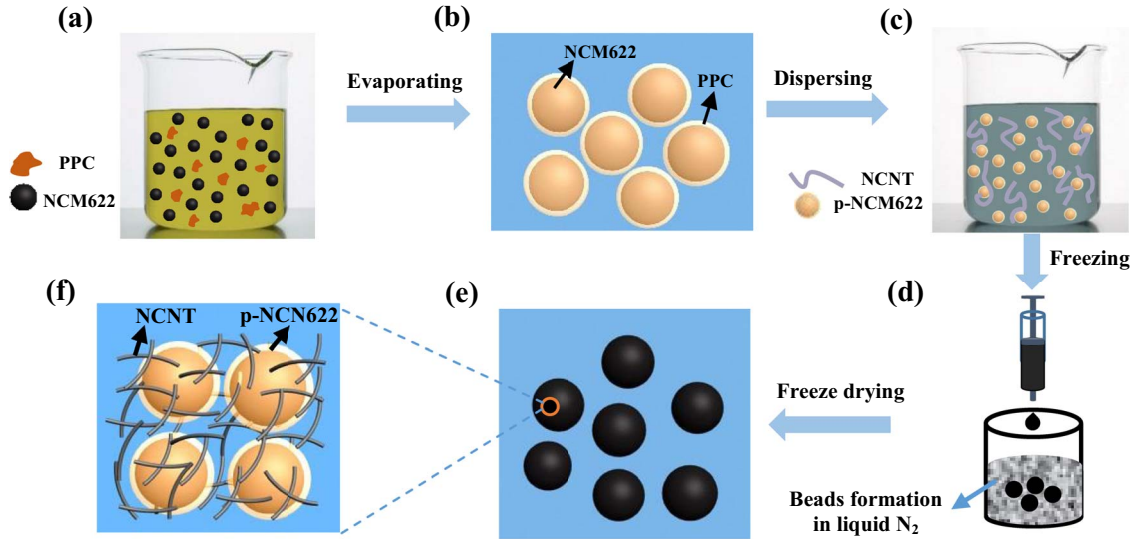

Figure 1. Schematic illustration of the synthesis process for the p-NCM622/NCNT composite: (a) The dispersion of NCM622 and PPC; (b) The PPC-coated NCM622 after evaporation of the solvent; (c) The dispersion of p-NCM622 and NCNT; (d) The freeze-casting process to form the p-NCM622/NCNT beads in liquid nitrogen; (e) The composites obtained after freeze-drying; (f) The partially enlarged region from (e), depicting the NCNT networks wrapped p-NCM622 composite.

precursor and LiOH (5% excess) were thoroughly mixed in an agate mortar. The mixture was firstly calcined at 550°C for 4 h in air, and then heated at 820°C for 12 h in an oxygen atmosphere to obtain the NCM622 powders.

The preparation of the p-NCM622/NCNT composite was carried out in accordance with the procedures shown in Figure 1. The PPC powder of 7.6 mg was dissolved in 10 mL acetone and then 380 mg NCM622 was added. The mixture was stirred at room temperature for 3 h, and then stirred at 60°C to evaporate the solvent, before drying in a vacuum oven at 80°C for 20 h. The obtained PPC-coated NCM622 (p-NCM622) powder was then added to a NCNT tert-butanol suspension (2 mg/mL), which was stirred for 15 min to obtain a uniform mixture. The mixture was then slowly dropped into liquid nitrogen using a pipette to form uniformly dispersed beads. Upon evaporation of liquid nitrogen, the collected beads were dried at −64°C for 48 h in a vacuum freeze dryer, to obtain the final p-NCM622/NCNT product for tests and analyses. In the p-NCM622/NCNT composite, the percentage of PPC coating is 2 wt% of the active material, and the percentage of NCNT is 5%. For comparison, the NCN622 modified with NCNT was also prepared by the same procedures for further characterization and measurements.

Structural characterization.—The crystal structures of the pristine and modified NCM622 materials were analyzed using X-ray powder diffraction (XRD, Xpert Pro MPD) with Cu Kα radiation (Kα = 0.15418 nm) between 10° and 80°. The morphologies were inspected on a scanning electron microscope (SEM, PHILIPS XL30 TMP, 15 kV). The microstructure of the samples were also checked by transmission electron microscopy (TEM, FEI Tecnai G20, 200 kV). The element distribution in the sample was measured by energy dispersive spectroscopy (EDS, OXFORD IET200).

Electrochemical measurements.—Electrochemical analyses of the samples were performed in the CR2032-type coin cells with a metallic lithium film as both the counter (negative) and reference electrodes. The electrolyte was 1.0 M $LiPF_6$ in mixed dimethyl carbonate (DMC)-ethylene carbonate (EC)-diethyl carbonate (DEC) soaked in a microporous polypropylene membrane separator (Celgard 2400). To fabricate the positive electrode, 70 wt% of the as-synthesized NCM662, 15 wt% of polyvinylidene difluorride (binder), and 15 wt% of the Super-P conductive carbon black were dispersed into an appropriate amount of N-methyl-pyrrolidone (NMP) and then stirred for 10 h on a magnetic stirrer to obtain a slurry, which was evenly coated on an Al foil and dried overnight at 100°C in vacuum. After that, the coin cells were assembled in an argon filled glove box.

Galvanostatic charge and discharge (GCD) tests were performed on the cells using the computer-controlled battery tester (Neware BTS, 5 V, 50 mA) between 2.80 and 4.25 V at different specific currents or mass normalized currents (against the total mass of active materials loaded on the positive electrode) at 25°C. An electrochemical workstation (Bio Logic VMP3) was used to study the cells by electrochemical impedance spectroscopy (EIS, amplitude: 10 mV; frequency range: 10 mHz to 100 kHz) and cyclic voltammetry (CV, voltage/potential range: 2.80 to 4.25 V; scan rate: 0.1 mV/s).

Results and Discussion

The obtained materials were subjected to morphology and structure characterization and electrochemical performance evaluation. X-ray diffraction patterns of the pristine NCM622, NCM622/NCNT and p-NCM622/NCNT are shown in Figure 2. There is no detectable impurity phase and all diffraction peaks match with those of the α-$NaFeO_2$ layered structure (R3m).[26] There is nearly no difference between the

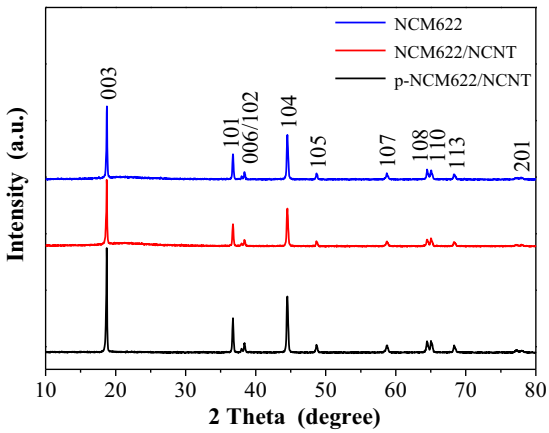

Figure 2. XRD patterns of NCM622, NCM622/NCNT and p-NCM622/NCNT.

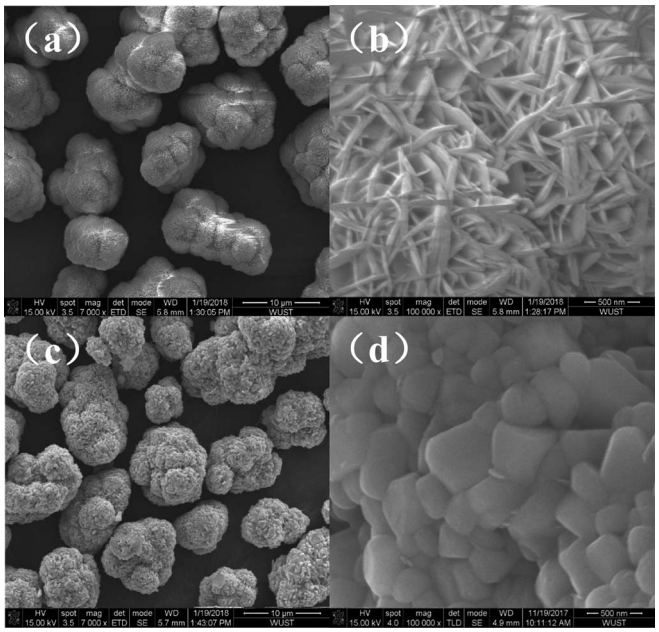

Figure 3. SEM images of (a, b) $Ni_{0.6}Co_{0.2}Mn_{0.2}(OH)_2$, (c, d) $LiNi_{0.6}Co_{0.2}Mn_{0.2}O_2$.

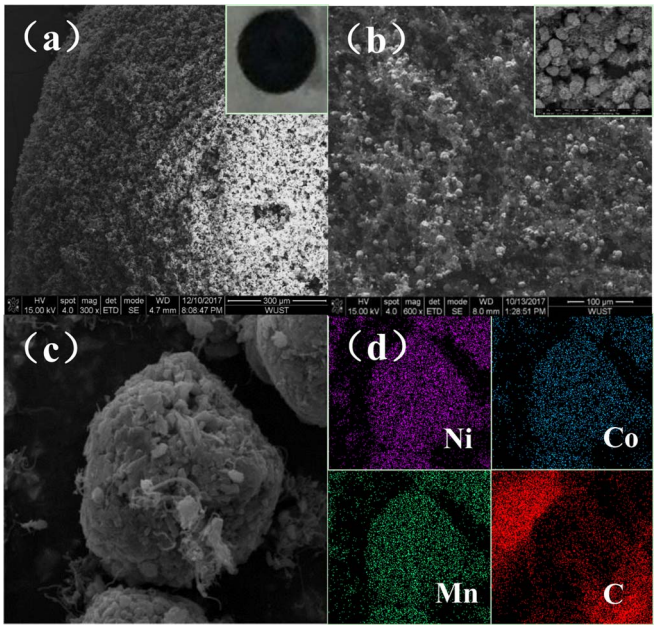

Figure 4. (a-c) SEM images of p-NCM622/NCNT. The insert in (a) is a digital photo of the freeze-dried bead, and the insert in (b) is a high magnification SEM image. (d) EDS elemental mappings corresponding to Ni, Co, Mn and C of (c).

three samples, demonstrating that the surface modification with PPC and NCNT does not change the crystal structure of the host electrode material. In general, the intensity ratio of I_{003}/I_{104} can be used to determine the degree of cation distribution in the crystal lattice, and it is greater than 1.2 for all the samples, indicating a low degree of cation mixing and lattice distortion. The clear split of the 006/102 and 108/110 peaks implies a well-developed hexagonal layered structure similar to that of the well-ordered α-$NaFeO_2$.[27,28]

The SEM images of the $Ni_{0.6}Co_{0.2}Mn_{0.2}(OH)_2$ precursor show irregular or pseudo-spheres of 8∼14 μm in size (Figure 3a), composed of loosely packed acicular primary particles (Figure 3b). After calcination, the secondary particle size and shape are basically retained (Figure 3c), but the primary particles entirely change to densely packed rhombic crystallites (Figure 3d). For comparison, Figures 4a–4d exhibit the SEM images of the p-NCM622/NCNT sample, and a digital photo of the formed composite bead with a size of ca. 4 mm (insert of Figure 4a). The NCNTs are intertwined with each other and the p-NCM622 microspheres are uniformly dispersed, forming a three-dimensional porous structure. Figure 4d displays results from EDS mapping, confirming the uniform distribution of Ni, Co and Mn in the p-NCM622/NCNT sample. More C is found around the pseudo-spheres than at the center, probably due to the PPC thin coating and the NCNT conductive networks around the particles.

Under high resolution TEM, the pristine NCM622 particle displays a round and smooth surface, as shown in Figure 5a. When loaded on the NCNT networks by the freeze-drying technique, the NCM622 particles are firmly attached with NCNTs. After the dual modifications, the TEM image of p-NCM622/NCNT reveals a 10 nm thick homogeneous coating of PPC on the surface of NCM622 and some NCNTs that are well connected (Figure 5b).

The unique structure of p-NCM622/NCNT as revealed by both SEM and TEM deserves more discussion. NCM622 and similar materials with good lithium storage capacities are often unable to deliver the expected discharge performance. This problem is known to mainly result from the intrinsically poor electronic and ionic conductivities of NCM622 that prevent the full material utilization. Whilst there are reported efforts in using carbon additives, such as CNTs and graphenes, to improve electron conduction, this approach does not help ion access to regions between the stacked particles. However, upon coating a thin layer of PPC on individual NCM622 particles, the regions between stacked particles become open to ion access. Thus, it is expected that the unique structure of p-NCM622/NCNT would benefit electron and ion conduction, and improve the discharge specific capacity and rate performance.

The electrochemical performance of the pristine and modified NCM622 positive electrode materials was evaluated at room temperature. Figure 6a presents the charge-discharge curves of the pristine NCM622, NCM622/NCNT and p-NCM622/NCNT at 0.1 C in the voltage range of 2.80 to 4.25 V. All the samples exhibit a diagonal voltage plateau from 3.60 to 4.25 V, and the specific discharge capacities of the pristine NCM622, NCM622/NCNT and p-NCM622/NCNT are 177.7, 185.4 and 201.3 $mAh \cdot g^{-1}$, respectively. These results demonstrate that the specific capacity of the PPC and NCNT modified NCM622 composites has been significantly improved. It can be attributed to the greatly enhanced ionic and electronic conductivities after coating PPC and wrapping NCNT on the NCM622 microspheres to form the three-dimensional porous composite structure.[29–31]

The formation of a transient cross-linking complex through the interaction of Li^+ and some carbonyl oxygen of PPC may enable faster migration of Li^+ than that coordinated with the ether chains.[32,23] The nitrogen doping can reduce the HOMO and LUMO energy levels of the graphitized CNTs and enhance the electron mobility in the conduction band, which significantly increases the electronic conductivity. In addition, the introduction of the nitrogen-containing functional groups with strong electron affinity can activate the surfaces of CNTs, increase the wettability and affinity of carbon nanotubes with the elec-

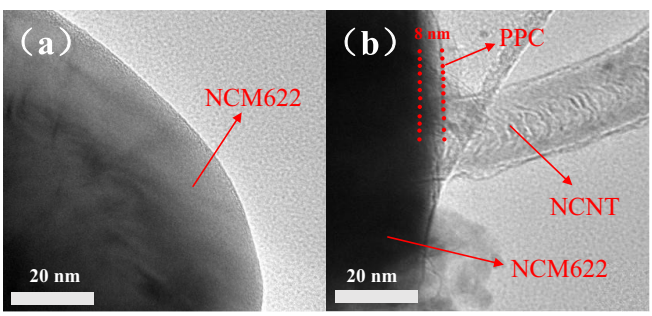

Figure 5. TEM images of (a) NCM622 and (b) p-NCM622/NCNT.

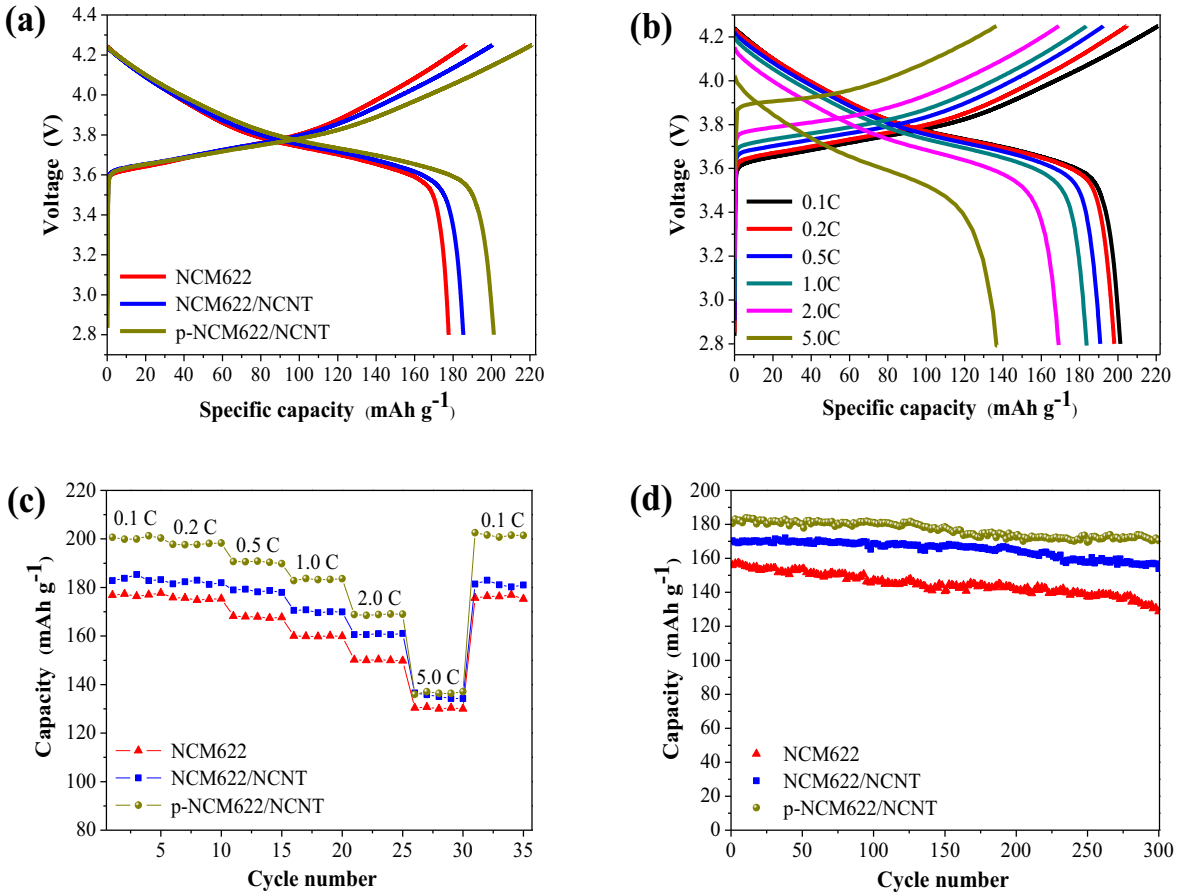

Figure 6. (a) Charge-discharge plots at 0.1 C for NCM622, NCM622/NCNT, and p-NCM622/NCNT; (b) Charge-discharge plots of p-NCM622/NCNT measured consecutively at the indicated increasing specific currents; (c) Rate capability, and (d) cycling performance for NCM622, NCM622/NCNT and p-NCM622/NCNT at the rate of 1.0 C.

trolyte, to further improve the lithium-ion transport/diffusion kinetics and enhance the approachability of the electrode materials.[24,33,34]

Figure 6b presents the charge-discharge profiles of p-NCM622/NCNT at various rates. The specific discharge capacities of p-NCM622/NCNT are determined to be 201.3, 198.1, 190.8, 183.7, 169.1 and 137.0 mAh·g^{-1} at 0.1, 0.2, 0.5, 1.0, 2.0, and 5.0 C, respectively. Figure 6c compares the rate capabilities of the three samples. As the discharging rate increases, the discharge specific capacity of all the three samples decreases, but the capacity of p-NCM622/NCNT remains higher than those of NCM622 and NCM622/NCNT at all rates applied. For instance, the discharge capacity of p-NCM622/NCNT is 169.1 mAh·g^{-1} at the rate of 2.0 C, much higher than 149.9 mAh·g^{-1} for NCM622. Though the p-NCM622/NCNT electrode displays greatly increased cycle performance and much higher discharge specific capacity within the rate range of 0.1 to 2.0 C, the higher rate capability advantage of the p-NCM622/NCNT composite tends to diminish at 5.0 C compared to NCM622/NCNT. This phenomenon is probably ascribed to the fact that the ion/electron conductor modified layered electrode materials here are relatively limited at high current densities, as the Li transport limitations may become pronounced, the Li diffusion coefficient may decrease rapidly due to the collapse of the interlayer spacing and the increased electrostatic repulsion between Li ions and the oxidized transitionmetal cations at rates higher than 5.0 C.[35] Further optimizations of the composition and structure, such as the ratio of NCM, PPC and NCNT, the thickness of PPC coating, and the size of the microsphere, would bring even higher rate performance. Figure 6d displays that the capacity retentions of cells with NCM622/NCNT and p-NCM622/NCNT are 90.42% and 94.40% after 300 cycles at 1.0 C, respectively, much higher than 82.60% of NCM622. The specific discharge capacity and the capacity retention of p-NCM622/NCNT (198.1 mAh·g^{-1} at 0.2 C, and 94.4% after 300 cycles at 1.0 C) are also higher than those of the typical NCM composites reported in the literature. For instance, the three-dimensional NCM523/MWCNT supramolecular assemblies (163.5 mAh·g^{-1} at 0.2 C, 74.0% after 300 cycles at 1.0 C),[36] the nano-polypyrrole coated NCM622 composite (155.9 mAh·g^{-1} at 0.2 C),[37] and the dual-conductive polymer modified NCM622 composite (184.3 mAh·g^{-1} at 0.2 C, 93.9% after 100 cycles at 0.5 C).[21]

The above reported results and analyses demonstrate convincingly that the dual- modification of NCM622 by PPC and NCNT has resulted in significant improvement in specific capacity, rate capability and cycling stability. Evidently, the dual modification was inter-particle in nature, leading to the three-dimensional porous composite electrode structure. The NCNT network provides sufficient electronic contacts between the NCM622 particles, facilitating charge transfer reactions. PPC is known to be a good conductor for lithium ions.[23] Thus, the PPC coating on each NCM622 particle prevents direct stacking between the particles, and enables lithium ions to access more reaction sites in the electrode. These two effects combine to reduce the electrode polarization reactions and improve the kinetic and rate performance of the electrode.[33,38,39] In addition, PPC is a Lewis base which is more likely to bond with the Lewis acid product (PF_5) from the possible decomposition of the electrolyte. The PPC coating may also help prevent attack of the electrode by HF probably formed during charging-discharging due to trace moisture in the cell. These protective functions of the PPC coating would hence help increase the cycle stability of the battery.[23] As the cycling performance of NCM is closely related to the structural stability and thermal stability, the PPC and NCNT co-modification may effectively delay the thermal decomposition of the $LiNi_{0.6}Co_{0.2}Mn_{0.2}O_2$ materials, reduce the heat generation due to the

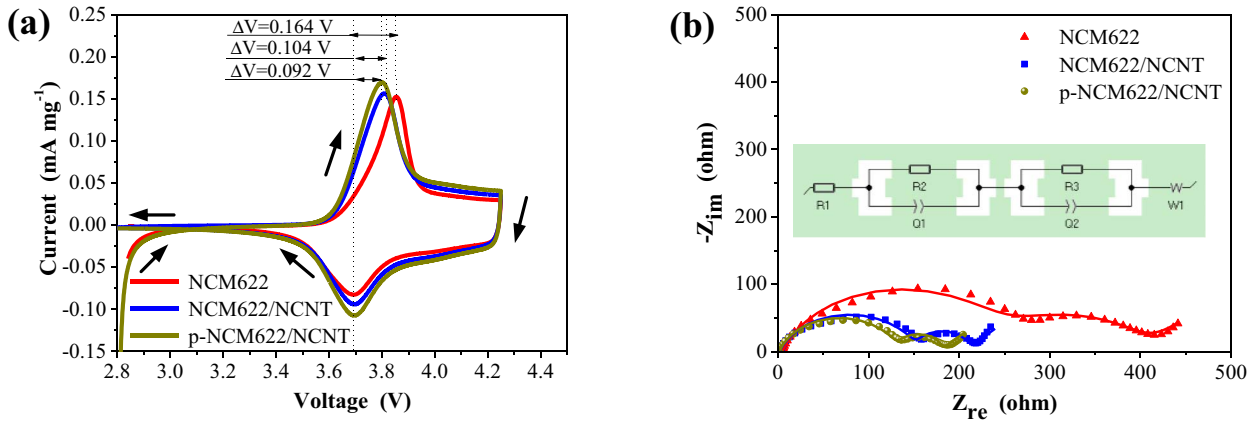

Figure 7. (a) Cyclic voltammograms (scan rate: 0.1 mV s^{-1}), and (b) electrochemical impedance plots of NCM622, NCM622/NCNT and p-NCM622/NCNT.

increase of the exothermic oxidation reaction temperature and block the release of oxygen from the nickel-cobalt-manganese ternary material particles, resulting in the greatly increased cycling stability of the p-NCM622/NCNT composite electrode.[40,41]

To further elucidate the enhancement of the electrochemical reversibility of the p-NCM622/NCNT electrode, cyclic voltammograms (CVs) of the cells were recorded between 2.80 and 4.25 V at a scan rate of 0.1 mV s^{-1}. As shown in Figure 7a, all of the three electrodes display a pair of redox peaks, which can be attributed to the insertion/extraction of lithium ions during charge-discharge, indicating absence of phase transition from hexagonal to monoclinic.[13,37] For the p-NCM622/NCNT electrode, the oxidation and reduction peaks appear respectively at 3.70 and 3.79 V. The potential gap is around 92 mV and which is much smaller than that of NCM622 (164 mV) and NCM622/NCNT (104 mV). This is evidence of improved electrochemical reversibility and lower polarization of p-NCM622/NCNT. Compared with the other two electrodes, the areas under redox peaks of the p-NCM622/NCNT electrode are much larger, confirming the substantially increased specific capacity of the dual modified composite due to the significantly increased reversibility and reactivity.

Electrochemical impedance spectroscopy (EIS) was applied to compare the charge transfer properties of NCM622, NCM622/NCNT and p-NCM622/NCNT. Figure 7b shows three features (or parts) on all the three impedance plots in addition to the high frequency intercept of each plot at the Zre axis that should have resulted from the total o resistance (Rs) of the electrolyte and the electrode. Decreasing the frequency leads to the appearance of two semicircles corresponding to the kinetic barriers at the interfaces. Its higher frequencies, the semicircle on the left is likely due to the transfer of Li^+ ions into the surface film (Rf) of NCM622. The semicircle in the mid-frequency region may correspond to the charge transfer between the electrolyte and electrode (Rct). The straight line in the low-frequency region seems to match the Warburg impedance (Zw).[19,42] The impedance spectra can be reasonably fitted using the equivalent circuit in the inset of Fig. 7b. The Rs Rf and Rct values of the p-NCM622/NCNT composites are derived to be respectively 1.67, 131.40 and 44.65 Ω cm^2, much smaller than those of the unmodified NCM622 material (4.35, 240.80 and 159.10 Ω cm^2). These results manifest that the PPC modification facilitates the ion transport, and the NCNT networks increase the electron conductivity of p-NCM622/NCNT, leading to the greatly reduced electrode and interfacial resistances for quicker and more complete charging and discharging.

Considering the possible particle separating effect of super P in the electrode, to further prove the function of PPC to increase the utilize areas that are blocked by particle stacking in pristine NCM, control experiments have been designed to replace PPC coating with the same weight percentage of super P. Namely, in the control electrode, the ratio of NCM622/NCNT, super P and PVDF was adjusted from 70:15:15 to 68:17:15 (the obtained sample was abbreviated as sp-NCM622/NCNT), the same ratio of NCM622-NCNT, PPC + super P and PVDF in the PPC and NCNT co-modification p-NCM622/NCNT composite electrode. The test results of sp-NCM622/NCNT are displayed in Figure S1. As shown in Figure S1a and b, the sp-NCM622/NCNT electrode displays discharge specific capacities of 185.9 mAh·g^{-1} at 0.1 C and 162.4 mAh·g^{-1} at 2.0 C, slightly higher than that of NCM622/NCNT (183.8 mAh·g^{-1} at 0.1 C and 160.6 mAh·g^{-1} at 2.0 C), but still much lower than the p-NCM622/NCNT composite electrode (201.3 mAh·g^{-1} at 0.1 C and 169.1 mAh·g^{-1} at 2.0 C), and the same trend is observed at the other test rates. The sp-NCM622/NCNT electrode also displays higher polarization and lower charge transfer ability compared to that of p-NCM622/NCNT (102 mV vs. 92 mV; 123.52 Ω cm^2 vs. 44.65 Ω cm^2), though a little improvement is observed in comparison to NCM622/NCNT (102 mV vs. 104 mV; 123.52 Ω cm^2 vs. 138.70 Ω cm^2), as shown in Figure S1c and d. These results indicate that the addition of PPC not only increases the utilization of the blocked area owing to particle stacking, but also effectively enhances the ionic conductivity of the NCM622 material.

From the above results and analyses, the unique inter-particle electronic and ionic modifications of NCM622 has proven to be effective for significant improvement in specific capacity, rate capability and cycling stability. As described in the schematic model shown in Figure 8, the mechanisms behind the observed electrochemical performance enhancement can be ascribed to several aspects: (1) The PPC coating offers high ionic conductivity and accelerates the lithium ion transport between the NCM622 microspheres and the electrolyte; (2) The surface PPC modification effectively enables ion access to regions between stacked NCM622 particles and reduces side reactions between the active materials and the electrolyte, and increases the electrochemical stability; (3) The three-dimensional interconnected porous NCNT networks provides fast electron transfer pathways; (4) The NCNT networks also increase the wettability of the electrolyte,[24] expand the electrode/electrolyte reaction interface and enhance the accessibility of the active materials.

Conclusions

We have synthesized a novel ion conductive PPC and electron conductive NCNT co-modified $LiNi_{0.6}Co_{0.2}Mn_{0.2}O_2$ electrode material using co-precipitation and the following coating and freeze-drying processes. The composite positive electrode material exhibits higher discharge specific capacity, rate performance and capacity retention in contrast to NCM622 and NCM622/NCNT. The PPC coating not only remarkably increases the ionic conductivity, but also effectively retards the corrosion and reduces the surface side reaction of the electrode materials. The NCNTs intertwine with each other to form a three-

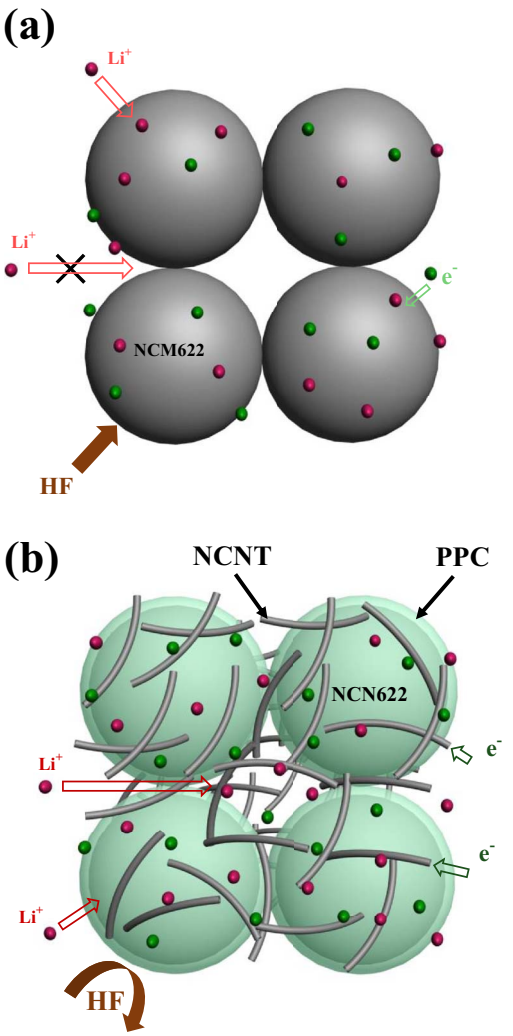

Figure 8. Mechanisms of the Li-ion/electron transport and the HF corrosion of (a) the un-modified NCM622, and (b) the co-modified p-NCM622/NCNT composite.

dimensional porous network structure, which improves the electronic conductivity and promotes charge transfer between the electrode/electrolyte interface. Therefore, the polarization of the electrode is greatly reduced and the kinetic process is improved. The unique composite structures are promising for application in lithium-ion power batteries and the facile strategy can be applied to synthesize other high-performance electrode materials.

Acknowledgments

This work was supported by the Natural Science Foundation of Hubei Province of China (No. 2013CFA021, 2018CFA022). GZC acknowledges the financial support from the Ningbo Municipal Government (3315 Plan) and the IAMET Special Fund (2014 A35001-1).

ORCID

Yingke Zhou https://orcid.org/0000-0002-6310-8831
George Z. Chen https://orcid.org/0000-0002-5589-5767

References

1. J. Lu, Z. Chen, Z. Ma, F. Pan, L. A. Curtiss, and K. Amine, *Nat. Nanotech.*, **11**, 1031 (2016).
2. B. Dunn, H. Kamath, and J.-M. Tarascon, *Science*, **334**, 928 (2011).
3. G. E. Blomgren, *J. Electrochem. Soc.*, **164**, A5019 (2017).
4. F. Schipper, E. M. Erickson, C. Erk, J.-Y. Shin, F. F. Chesneau, and D. Aurbach, *J. Electrochem. Soc.*, **164**, A6220 (2017).
5. A. Manthiram, J. C. Knight, S.-T. Myung, S.-M. Oh, and Y.-K. Sun, *Adv. Energy Mater.*, 6 (2016).
6. Y. Shi, M. H. Zhang, C. C. Fang, and Y. S. Meng, *J. Power Sources*, **394**, 114 (2018).
7. Y. Shi, M. H. Zhang, Y. S. Meng, and Z. Chen, *Adv. Energy Mater.*, **9**, 9 (2019).
8. H. Li, M. Cormier, N. Zhang, J. Inglis, J. Li, and J. R. Dahn, *J. Electrochem. Soc.*, **166**, A429 (2019).
9. J. Meng, H. Guo, C. Niu, Y. Zhao, L. Xu, Q. Li, and L. Mai, *Joule*, **1**, 522 (2017).
10. J. Sicklinger, M. Metzger, H. Beyer, D. Pritzl, and H. A. Gasteiger, *J. Electrochem. Soc.*, **166**, A2322 (2019).
11. M. Dong, Z. Wang, H. Li, H. Guo, X. Li, K. Shih, and J. Wang, *Acs Sust. Chem. Eng.*, **5**, 10199 (2017).
12. J.-Z. Kong, S.-S. Wang, G.-A. Tai, L. Zhu, L.-G. Wang, H.-F. Zhai, D. Wu, A.-D. Li, and H. Li, *J. Alloys Compd.*, **657**, 593 (2016).
13. K. Liu, G.-L. Yang, Y. Dong, T. Shi, and L. Chen, *J. Power Sources*, **281**, 370 (2015).
14. E. Han, X. Liu, L. Zhu, C. Pan, and Z. Wu, *Ionics*, **19**, 997 (2013).
15. K. Min, K. Park, S. Y. Park, S.-W. Seo, B. Choi, and E. Cho, *J. Electrochem. Soc.*, **165**, A79 (2018).
16. G. Dai, H. Du, S. Wang, J. Cao, M. Yu, Y. Chen, Y. Tang, A. Li, and Y. Chen, *Rsc Adv.*, **6**, 100841 (2016).
17. X. Jiang, Z. Yuan, J. Liu, X. Jin, L. Jin, P. Dong, Y. Zhang, Y. Yao, Q. Cheng, C. Liu, Y. Zhang, and X. Yu, *Int. J. Electrochem. Sci.*, **13**, 2341 (2018).
18. K.-S. Park, S. B. Schougaard, and J. B. Goodenough, *Adv. Mater.*, **19**, 848 (2007).
19. K.-S. Lee, Y.-K. Sun, J. Noh, K. S. Song, and D.-W. Kim, *Electrochem. Commun.*, **11**, 1900 (2009).
20. D. Lepage, C. Michot, G. Liang, M. Gauthier, and S. B. Schougaard, *Angew. Chem., Int. Ed.*, **50**, 6884 (2011).
21. S. H. Ju, I.-S. Kang, Y.-S. Lee, W.-K. Shin, S. Kim, K. Shin, and D.-W. Kim, *Acs Appl. Mater. Interfaces*, **6**, 2546 (2014).
22. Y.-S. Lee, W.-K. Shin, A. G. Kannan, S. M. Koo, and D.-W. Kim, *Acs Appl. Mater. Interfaces*, **7**, 13944 (2015).
23. D. Zhou, R. Zhou, C. Chen, W.-A. Yee, J. Kong, G. Ding, and X. Lu, *J. Phys. Chem. B*, **117**, 7783 (2013).
24. X. Tu, Y. Zhou, X. Tian, Y. Song, C. Deng, and H. Zhu, *Electrochim. Acta*, **222**, 64 (2016).
25. X. Tu, Y. Zhou, and Y. Song, *Appl. Surf. Sci.*, **400**, 329 (2017).
26. J.-W. Choi and J.-W. Lee, *J. Power Sources*, **307**, 63 (2016).
27. K. J. Kim, Y. N. Jo, W. J. Lee, T. Subburaj, K. Prasanna, and C. W. Lee, *J. Power Sources*, **268**, 349 (2014).
28. Y. Chen, Y. Zhang, B. Chen, Z. Wang, and C. Lu, *J. Power Sources*, **256**, 20 (2014).
29. J. Zhang, J. Zhao, L. Yue, Q. Wang, J. Chai, Z. Liu, X. Zhou, H. Li, Y. Guo, G. Cui, and L. Chen, *Adv. Energy Mater.*, 5 (2015).
30. X. Tian, Y. Zhou, X. Tu, Z. Zhang, and G. Du, *J. Power Sources*, **340**, 40 (2017).
31. G. Du, Y. Zhou, X. Tian, G. Wu, Y. Xi, and S. Zhao, *Appl. Surf. Sci.*, **453**, 493 (2018).
32. Y. Tominaga, K. Yamazaki, and V. Nanthana, *J. Electrochem. Soc.*, **162**, A3133 (2015).
33. W. H. Shin, H. M. Jeong, B. G. Kim, J. K. Kang, and J. W. Choi, *Nano lett.*, **12**, 2283 (2012).
34. B. Xiong, Y. Zhou, R. O'Hayre, and Z. Shao, *Appl. Surf. Sci.*, **266**, 433 (2013).
35. M. D. Radin, S. Hy, M. Sina, C. C. Fang, H. D. Liu, J. Vinckeviciute, M. H. Zhang, M. S. Whittingham, Y. S. Meng, and A. Van der Ven, *Adv. Energy Mater.*, **7**, 1602888 (2017).
36. D.-W. Kim, N. Zettsu, and K. Teshima, *J. Mater. Chem. A*, **5**, 22797 (2017).
37. M.-R. Shin, J.-T. Son, and J. Nanosci, *Nanotech.*, **17**, 8869 (2017).
38. Z. Wu, X. Han, J. Zheng, Y. Wei, R. Qiao, F. Shen, J. Dai, L. Hu, K. Xu, Y. Lin, W. Yang, and F. Pan, *Nano lett.*, **14**, 4700 (2014).
39. Y. Zhou, J. Lu, C. Deng, H. Zhu, G. Z. Chen, S. Zhang, and X. Tian, *J. Mater. Chem. A*, **4**, 12065 (2016).
40. J.-H. Shim, Y.-M. Kim, M. Park, J. Kim, and S. Lee, *ACS Appl. Mater. Interfaces*, **9**, 18720 (2017).
41. G. Wu and Y. Zhou, *J. Energy Chem.*, **28**, 151 (2019).
42. N. Laszczynski, S. Solchenbach, H. A. Gasteiger, and B. L. Lucht, *J. Electrochem. Soc.*, **166**, A1853 (2019).